TASK QUARTERLY 12 No 3, 185–195

PERFORMANCE OF THREE TURBULENCE MODELS IN 3D FLOW INVESTIGATION FOR A 1.5-STAGE TURBINE

MACIEJ KARCZEWSKI AND JAROSŁAW BŁASZCZAK

Technical University of Lodz, Institute of Turbomachinery,
Wólczańska 219/223, 93-005 Lodz, Poland
maciej.karczewski@p.lodz.pl

(Received 7 May 2008; revised manuscript received 12 June 2008)

Abstract: The object of this study was to investigate the flow phenomena in a cold air turbine built at the Institute of Jet Propulsion and Turbomachinery at Aachen Technical University (IST RWTH Aachen, Germany). The said turbine had been studied previously both experimentally and numerically on an IST's flow solver called *Panta Rhei*. Since that time certain improvements, computational-wise, have been implemented in the code. In order to test them, new simulation runs were conducted. The detailed studies of the measured and computed flow angles as well as a flow velocity analysis are the means for this evaluation.

Keywords: turbulence modeling, numerical research, low-pressure turbine

1. Introduction

The extensions to the existing turbulence models as well as the instalment of a robust flow transition prediction scheme in *Panta Rhei* code, revitalized the idea of researching the performance of 3 turbulence models (Chien's k-ε, k-ω of Wilcox, and Menter's Shear Stress Transport) in rendering the flow structures inside the IST RWTH turbine. However, the research area was narrowed to the 1st stator only. In comparison to older numerical studies, new simulations were realized on an improved grid, having an additional inflow block and a concentrated wake line. The results were compared to the experiment in [1].

2. Turbine test rig

The IST RWTH turbine rig is conventionally equipped (compare *i.e.* with [2]). Hence, before entering the flow channel, air travels through the honey-combed silencer, the number of shaft revolutions is controlled by an eddy-current brake, while custom-made rings permit measurements in four planes:

(i) plane 0–143 mm before the 1st stator row;
(ii) plane 1–15 mm in front of the rotor leading edge (LE);
(iii) plane 2–8 mm behind the rotor trailing edge (TE);

(iv) plane 3–8 mm behind the 2nd stator.

Figure 1 shows these sections more precisely. In 1999, the turbine test bed was equipped with a probe that was measuring the total pressure and temperature values in plane 0 that, along with the static pressure readings taken in the same position, were used to determine the mass flow rate (see [1]).

The stator vanes of this turbine are based on the Traupel's profile, while the rotor blade resembles the profile of the Von Karman Institute. Blades are untwisted and have constant cross-sections height-wise. Table 1 presents the main geometrical data relevant to this turbine.

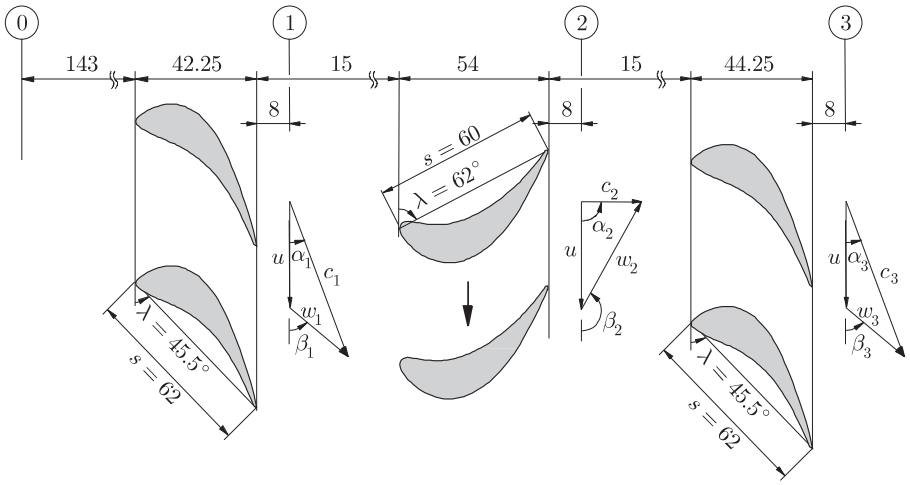

Figure 1. Definition of velocity triangles and flow angles;
$\alpha_1 = 20°$, $\beta_1 = \alpha_{1\mathrm{rel}} = 49.3°$, $\alpha_2 = 90°$, $\beta_2 = \alpha_{2\mathrm{rel}} = 151.2°$, $\alpha_3 = 20°$, $\beta_3 = \alpha_{3\mathrm{rel}} = 49.3°$

Table 1. Geometrical data of the IST turbine

		1st and 2nd stator Traupel's profile	Rotor mod. VKI profile
Hub diameter	d_{hub}	490 mm	490 mm
Tip diameter	d_{cas}	600 mm	599.2 mm
Passage height	H	55 mm	55 mm
Tip clearance height	Δ	–	0.4 mm
Height/chord ratio	H/l_s	0.887	0.917
Number of blades	z	36	41
Blade pitch	BP	10°	8.78°

An electronic data acquisition process, employed for the experimental campaigns at IST, used one of the probes, permanently attached to the hub and rotated by 20° in the circumferential direction, to establish the point of the machine's nominal operation (3500 rpm), coincident with Mach number $\mathrm{Ma}_1 = 0.449$. For the study found in [1], 21 radial and 25 circumferential probe positions were measured. More details on the numerical and empirical research activities undertaken at IST RWTH Aachen can be found in the literature [1, 3, 4].

3. *Panta Rhei* – numerical platform for computations

The *Panta Rhei* code belongs to a group of Reynolds- and Favre-averaged Navier-Stokes (RANS) flow solvers. It consists of three software components – the mesh tool *Frame*, the flow solver *Panta*, and the post-processor *Treat*. More information on this software platform is available in [5].

In this solver the vector fluxes (entering and leaving the finite volume) are computed directly at the walls. The upwind scheme algorithm [6] determines the Euler fluxes, whereas the viscous fluxes are computed with the help of asymmetrical interpolation [7]. All numerical simulations for the purposes of this campaign were realized implicitly.

4. Turbulence modelling

During every iteration the following set of RANS equations is solved [8]:

$$\frac{\partial \bar{\rho}}{\partial t} + \frac{\partial \bar{\rho}\tilde{c}_i}{\partial x_i} = 0, \tag{1}$$

$$\frac{\partial \bar{\rho}\tilde{c}_i}{\partial t} + \frac{\partial \bar{\rho}\tilde{c}_i\tilde{c}_j}{\partial x_j} + \frac{\partial \bar{p}}{\partial x_i} + \frac{\partial}{\partial x_j}\left(-\tilde{\tau}_{ij} + \bar{\rho}\tilde{c}_i''\tilde{c}_j''\right) = 0, \tag{2}$$

$$\frac{\partial \bar{\rho}\tilde{E}}{\partial t} + \frac{\partial \bar{\rho}\tilde{c}_i\tilde{E}}{\partial x_j} + \frac{\partial \tilde{c}_i\bar{p}}{\partial x_i} + \frac{\partial}{\partial x_j}\left(-\tilde{c}_j\tilde{\tau}_{ij} + \bar{\rho}\tilde{c}_j\tilde{c}_i''\tilde{c}_j'' + \bar{\rho}\tilde{c}_i''\tilde{h}'' + \lambda\frac{\partial \bar{T}}{\partial x_i}\right) = 0, \tag{3}$$

$$c = f(u,v,w), \quad \tilde{E} = \tilde{e}_{\text{in}} + \frac{\tilde{c}_i\tilde{c}_i}{2} + \frac{\tilde{c}_i''\tilde{c}_i''}{2}, \quad \text{Pr} \equiv \frac{c_p\mu}{\lambda}. \tag{4}$$

Although the *Panta* code offers several other robust techniques of turbulence modeling, including the Explicit Algebraic Reynolds Stress Model (EARSM, see [9]), this study has been focused on three different two-equation turbulence models:

(1) k-ε model of Chien;
(2) k-ω model by Wilcox;
(3) Shear Stress Transport (SST) model of Menter.

It is believed that the k-ε model proves to be very useful in simulations of flows in outer regions, whereas the k-ω model performs strongly in rendition of turbulent effects in vicinities of the endwalls. Finally, the last model, SST, is a combination of the previous two models. In general, it uses the k-ε model equations for the outer region turbulence and the k-ω formulations for the phenomena occurring near the walls. Literature positions [8, 10–12] broadly introduce each model, while [13] lists model equations and constants.

5. Meshing, convergence, and boundary conditions

A structured O-3D grid was developed in order to simulate airflow through the 1st stator of the IST axial turbine. This kind of mesh topology proves useful in netting blade profiles with strong curvatures, just as the one in the tested vane.

The mesh used for this study consisted of over 550 000 nodes, k-direction corresponding with the height of the channel. Figure 3 below presents the 3D grid used for the study along with the cross-section at the plane $k = 30$.

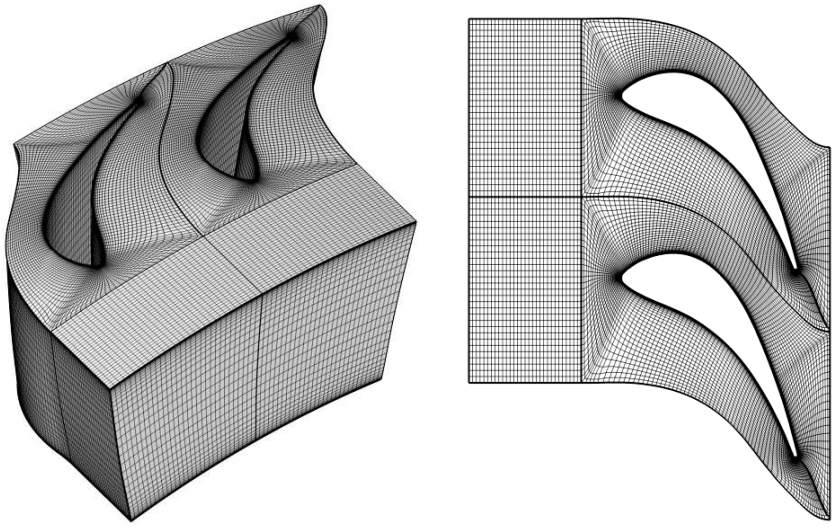

Figure 2. Computational grid: 3D view and cross-section

All simulations were launched on the distributed RWTH Sun SMP cluster. 20 Sparc processors solved each problem needing around 30 s to perform one iteration. Table 2 shows the computed mass flow rates at the inflow and outflow by model along with the amount of numerical steps required to reach a solution.

Table 2. Inflow and outflow mass flow rates and their variation from arithmetic mean

	Inflow [kg/s]	Outflow [kg/s]	Variation [%]
k-ε Chien (>14 000 iter.)	7.4821	7.4887	0.0882
k-ω Wilcox (≈14 000 iter.)	7.5059	7.5127	0.0906
SST (>4 000 iter.)	7.4976	7.5007	0.0413

The differences are minimal with SST delivering the best convergence. In 1999, the test rig lacked Venturi tube and precise measurements of mass flow rate could not be taken. The research in [3] reports for this machine a mean value of about 7.3 kg/s. When compared with the estimates in Table 2, this amount shows that all numerical simulations came close to the experimental data.

For computations presented herein, the mixing length was specified to be $l_t = 0.275$ mm (k-ε Chien and SST), whereas for k-ω Wilcox $l_t = 0.0275$ mm. The boundary layer (BL) thickness was assumed to be 2.75 mm for the hub and 6.60 mm for the casing as per [14]. Table 3 lists the remaining boundary conditions.

Table 3. Numerical boundary conditions assumed for all tested models

Inflow (in front of 1st stator – plane 0)	Outflow (behind 1st stator – plane 1)
$P_{\mathrm{tot}}(r)$, mean $P_{\mathrm{tot}} = 153\,700$ [Pa] $T_{\mathrm{tot}}(r)$, mean $T_{\mathrm{tot}} = 308$ [K] $\alpha = 0$ [°] Ma = 0.135 [-] Tu = 2 [%]	$P_{\mathrm{sta}}(r)$, mean $P_{\mathrm{sta}} = 134\,209$ [Pa]

6. Presentation of the results

In the following section, the pitchwise, α, as well as spanwise, γ, flow angles are studied. In the experiment conducted by [1], the former is defined as the angle between the meridional direction (0°) that, here, happens to coincide with the machine axis, and the projection of the absolute velocity vector $\vec{c}$ onto the axial plane. The positive angles are rotated away from the turbine axle. The spanwise angle on the other hand, is an angle between the said projection and the absolute flow velocity $\vec{c}$. Positive angles point towards the casing. Figure 3, where a 5-hole pressure probe with the NTC element, (left to the phrase "T_{probe}") is depicted, clarifies this.

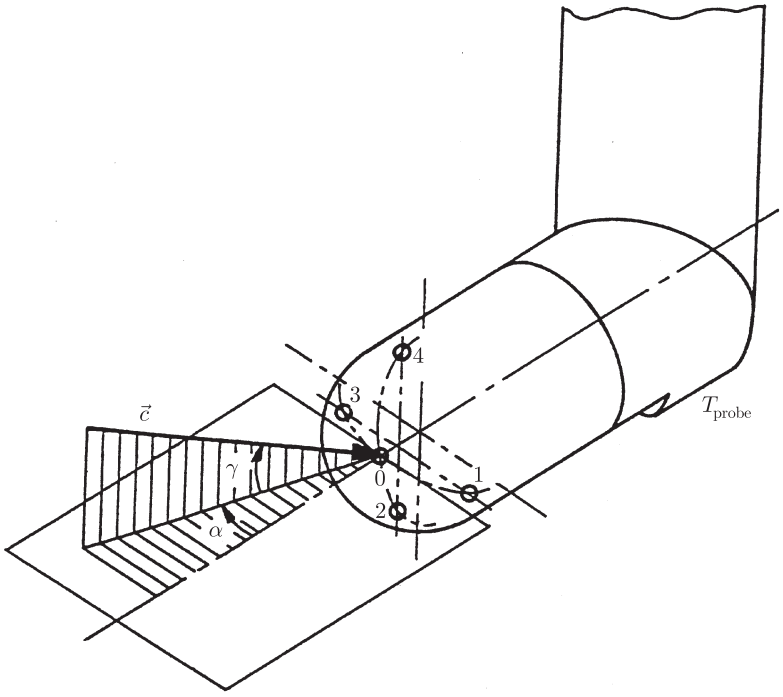

Figure 3. Experimental measurement of flow angles [1]

Figure 4 below presents the topographical distribution of the flow angle α. In general, the angle maximum and minimum have been numerically rendered in correct locations. The k-ω model by Chien satisfactorily arrives at the angle minimum, but overpredicts its value, while the SST model comes closest to the real magnitude. Additionally, the lower passage vortex, indicated by locally steep gradients of alpha, has been also recognized in all three cases. This ends however, the similarities between the experiment and numerical simulations. On the contrary, in the empirical test, the area between upper and lower passages of the horseshoe eddy is a flow decisively assuming a circumferential direction, whereas in computations the material in this region is carried rather axially.

These differences are clearer on the graph seen in Figure 5. The plot shows that the angle maximum near the hub has been predicted well, although the computed values have reached higher levels than in the experiment performed in [1]. Near the

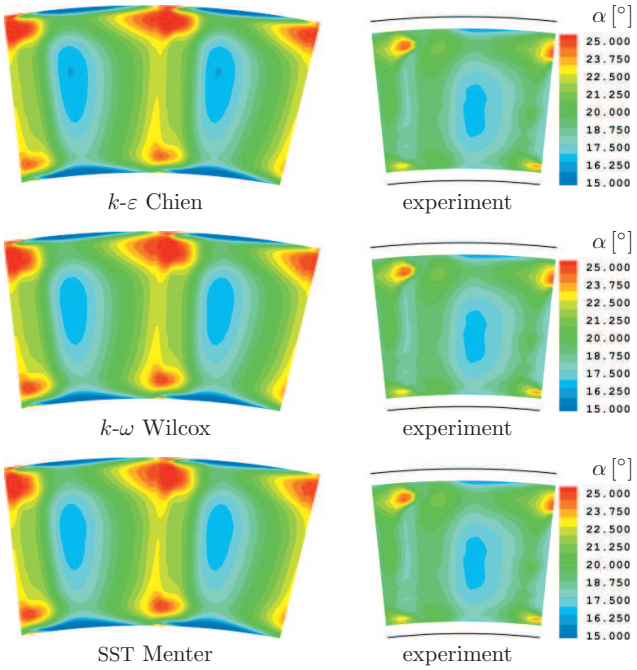

Figure 4. Contour plots of pitchwise flow angle α at the stator outlet ($X = 0.074\,\mathrm{m}$)

shroud, a completely different angle distribution can be observed with a maximum at about 90% of the height. This finds no reference in the experiment. The values of the angle have been also overestimated but the shapes are similar.

To better understand the poor rendition of the top portion of the radial distribution of α, two earlier experimental studies, supported by the numerical research of the same turbine, are presented. The massflow-averaged flow angles seen in Figure 6 have been gathered from the computations and experiments made by Gallus [15] and Volmar [4], respectively.

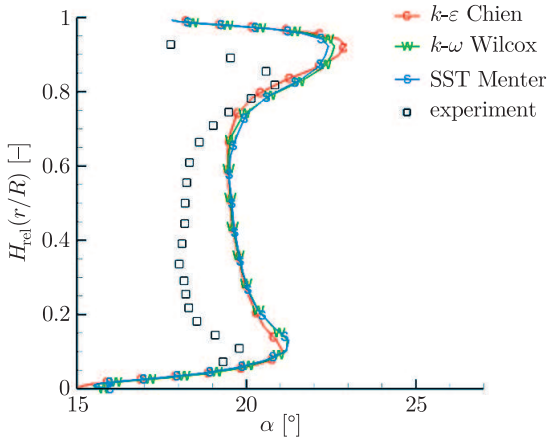

Figure 5. Radial distribution of the pitchwise angle α (axial station $X = 0.074\,\mathrm{m}$)

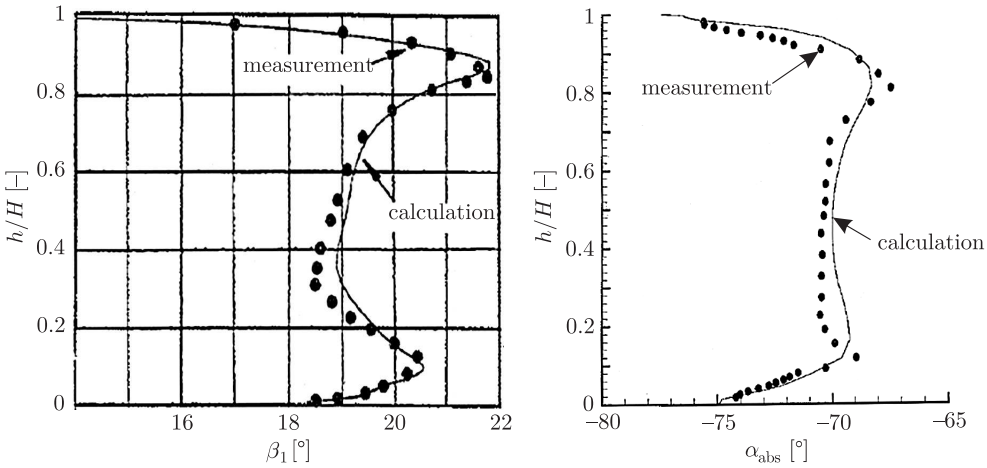

Figure 6. Distribution of the pitchwise angle – Gallus [15] (left) and Volmar [4] (right); the symbols α and β_1 refer to the same quantity

Different values of α in the plot on the right are in fact identical to those found in the picture on the left. This becomes clear when the angles are shifted by 90° (differences are due to the coordinate system chosen). It is apparent that, in case of the study in [15], the agreement between experimental data and simulation is rather high. The picture on the right was an unsteady computation of the whole turbine, where slightly different boundary conditions (and most notably boundary layers) were provided. Namely 3 mm was the thickness given at the hub and 4 mm at the shroud, following the measurements made by Walraevens presented in [16].

The precise data for the test case presented on the left hand side is not available. There however, [15] used computational software developed by the University of Stuttgart in a steady state calculation of the entire stage, empirically investigated by [17]. Although quite similar experimentally measured pitchwise angle profiles are depicted on all three plots, only two of the computations match the factual distribution. The numerical simulation presented herein is visibly the poorest of all. The reason behind it is attributed to the over-assumption of the boundary layer at the shroud, which was set to 6.60 mm compared to 4.00 mm in Volmar's numerical study (see [4]). Another probable drawback was the provision of a completely incidence-free ($\alpha = 0°$) inflow at the turbine inlet, where, in fact, for example [18] measured it to be about 3°. In the two earlier computations, shown in Figure 6, exactly such values were assumed.

The comparison of the γ angle between the experiment and computation also draws attention to some disproportions. Two local maxima are visible in the experimental contour (Figure 7) and massflow-averaged plots (Figure 8).

The contour plots show them at the suction side near the trailing edge region. The maximum near the casing approaches 7° and is much higher than the maximum at the hub. Yet again, this can be explained by the greater thickness of the boundary layer at the shroud. Thermann in [19] explains that the error in mathematical derivation of the boundary layer can be influenced by the gradients of velocity at the turbine inlet. Since this machine stand was laden with quite high massflow and rotational speed

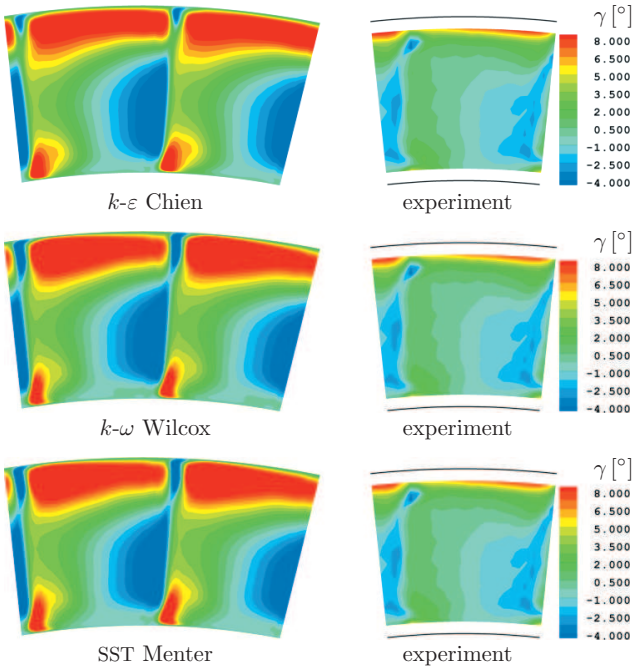

Figure 7. Distribution of the γ flow angle at the stator outlet ($X = 0.074\,\mathrm{m}$)

fluctuations at the turbine inlet (see Sections 5.3 and 6.2 in [13]), it is very probable that the real thickness of the boundary was in fact smaller.

Yet another reason is given in [20]. The steep γ gradients result also from the limitations of the measurement technique. The introduction of the probe into the endwall region behind the first stator, where the flow undergoes separation, causes a rapid acceleration of the travelling medium around the body of the probe. Additionally, the bore located above, through which the probe has to be slipped inside the turbine passage, itself disturbs the layers of travelling air. The fluid is dragged upward and that is detected by the measuring equipment as an increasingly radial flow.

The same radial scheme is found in the computations, partly due to a rapid increase in the static pressure that existed inside the flow channel (from hub to casing difference of 4 000 Pa). Such pressure rise can be explained by the quasi-narrowing of the passageway due to the interacting boundary layer material that, moving upward, unites with the air masses traveling in the freestream area. This leads to an increase in velocity and, in effect, creation of secondary flows [21]. Another reason is the lack of transition modelling in all simulations. The flow was assumed to be fully turbulent across the whole passage, but this is not likely in reality.

In fact, the low-Re-number turbomachinery flows are highly separating, especially in areas near hubs and shrouds. The influence of the separation on the mainstream flow is even greater when geometries with low blade height-to-chord ratios are considered [19]. Since in the case of Traupel's profile of the Aachen's turbine this ratio is below 1, the effects of separation are potentially high. They are not modelled

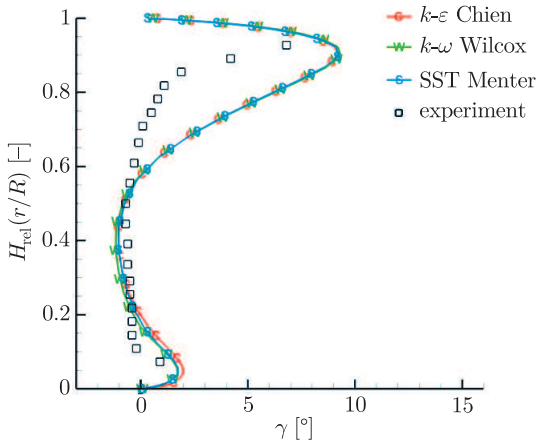

Figure 8. Radial distribution of the spanwise angle (axial station $X = 0.074\,\mathrm{m}$)

though, what could certainly lead to misrepresentation of the flow angles in the upper portion of the flow channel.

7. Integral averaging – comparison

Table 4 below outlines the integrally averaged parameters coming from numerical simulations and the experiment. The values were mass flow-averaged in the circumferential direction and averaged over the area represented by the relative height of the flow channel. The pitchwise and radial angles as well as the absolute, axial, tangential, and radial velocities are presented.

Table 4. Integral averages of the characteristic flow parameters; for starred values – $X = 0.074\,\mathrm{m}$

	α [°]	γ [°]	c_{abs} [m/s]	c_{ax} [m/s]	c_{tan}[m/s]	c_r [m/s]
k-ε C	20.18*	2.23*	149.510	51.370	140.090	3.950
k-ω W	20.26*	2.15*	149.370	51.480	139.910	3.850
SST	20.24*	2.18*	149.230	51.410	139.790	3.870
exp.	18.80	0.40	148.903	47.884	140.836	0.985

When compared to the experiment, the numerical simulations of the α angle show how close *Panta Rhei* came to the design condition (compare with turbine geometrical data in Figure 1), where the α value of 20° was planned. The measured data differs here to a greater extent. Walraevens in [18] attributed this difference to the upstream influence of the rotor.

The same cannot be said about the radial angle γ, where variations between experiment and numerical investigations are slightly bigger. This time, the departure from the blueprint value ($\gamma = 0°$) proves disadvantageous to *Panta Rhei*, what, naturally, explains the differences in the axial and radial velocity components, seen in the next columns. Despite of it, the agreement between the tangential velocity components is remarkable.

The radial velocity component, c_r, is expected to be 0, but the integral average of this parameter is equal to about 4 m/s in computations and almost 1 m/s in

the experiment. This suggests that the layers of flow travel towards the casing. However, measurements recorded in [1] behind the second stator show that the flow assumes an opposite direction and "returns" towards the hub. Unfortunately, no pressure measurements at the first stator vane profile were registered. Such dataset could potentially indicate regions where the flow separated from the wall and aid in understanding this upward movement behind the stator.

Generally, the simulations have delivered results that remain in quite good agreement with the real flow. This fact suggests that a steady state numerical computation of flows in single-stator configurations can be an accurate tool in predicting the turbine behavior.

8. Final remarks

A detailed analysis of the flow fields showed that the estimations of flow angles were influenced by the definition of boundary layer (BL) zones. To derive the BL thickness, [15] used mathematical models, basing on own measurements of inflow velocity. This approach was deemed accurate in later research attempts including [1]. As it turned out, such methodology omitted few essential flow facts pertinent to this turbine. In an attempt to remain as close as possible to the experimentally measured conditions, these BL values were utilized in the present numerical study. Such approach, after all, proved to be disadvantageous.

Another remark points to a need of developing less invasive methods of experimental measurement. The equipment introduced into a flow channel can cause disruptions of the current that result in an inaccurate detection of the characteristic parameters. A good example is the elevated pressure level recorded and, at the same time, caused by the probe located behind the first stator. This, in turn, contaminated the results of numerical simulations when these unlikely readings were introduced into *Panta Rhei* as boundary conditions. Although certain high-precision least-invasive methodology, such as Laser Doppler Anemometry (LDA), has been already in use, the costs associated with this approach are much higher than in case of 5-hole pressure probes. Likewise, the use of probes does not necessarily have to burden the flow measurements with error, when an appropriate mathematical correction of measured data is used.

Finally, as to the performance of the three studied models, SST cannot be singled out as the one coming definitely closest to the experimental findings. The differences between all models were not large and, hence, the choice of the model should always be based on the objectives of numerical research.

References

[1] Ernst M, Reinmöller U and Gallus H E 1999 *Untersuchung von Clocking-Effekten in einer $1\frac{1}{2}$-stufigen Axialturbine*, Studienarbeit RWTH Aachen
[2] Blaszczak J R 2005 *ASME Paper* **GT2005–68833**
[3] Reinmöller U, Stephan B, Schmidt S and Niehuis R 2002 *J. Turbomachinery* **124** (1) 52
[4] Volmar T W, Brouillet B C, Gallus H E and Benetschik H 1998 *AIAA Paper* **98–3247**
[5] Thermann H, Schmidt S., Weiß C and Niehuis R 2001 *TASK Quart.* **5** (4) 537
[6] Roe P L 1981 *J. Comp. Phys.* **043** 357
[7] Chakravarthy S R 1988 *High Resolution Upwind Formulations for the Navier-Stokes Equations*, in: Von Karman Institute for Fluid Dynamics – Lecture Series **5**

[8] Wilcox D C 1993 *Turbulence Modelling for CFD*, DCW Industries: La Cañada C, United States
[9] Wickerath B and Niehuis R 2006 *A Study of Nonlinear Eddy Viscosity Models in a Flow Solver for Turbomachinery*, ICAS Conference, Hamburg, Germany **ID 717**
[10] Chien K Y 1982 *AIAA J.* **029** (2) 33
[11] Menter F R 1993 *AIAA Paper* **93–2906**
[12] Menter F R and Rumsey C L 1994 *AIAA Paper* **94–2343**
[13] Karczewski M 2007 *Advanced Numerical 3D Flow Investigation in a 1.5-stage Low-pressure Turbine*, Diploma Thesis, TU Lodz, Poland
[14] Zeschky J and Gallus H E 1991 *Experimentelle Untersuchung der dreidimensionalen Rotorströmung einer axialen Kaltluftturbine*, Dissertation, RWTH Aachen
[15] Gallus H E, Zeschky J and Hah C 1994 *ASME Paper* **94-GT-143**
[16] Walraevens R E and Gallus H E 1996 *AGARD Conference Proceedings 571, Loss Mechanisms and Unsteady Flows in Turbomachines*, Paper 39
[17] Zeschky J and Gallus H E 1993 *ASME* **115** 128
[18] Walraevens R E, Gallus H E and Bohn D 2000 *Experimentelle Analyse dreidimensionaler instationärer Strömungseffekte in einer $1\frac{1}{2}$-stufigen Axialturbine*, Dissertation, RWTH Aachen, VDI Verlag: Düsseldorf
[19] Thermann H 1998 *Untersuchung und Bewertung algebraischer Transitionsmodelle in Turbomaschinen*, Diplomarbeit, RWTH Aachen
[20] Reinmöller U, Büscher C, Große-Laxzen R and Zachau U 2001 *Clocking – Messungen an der Kaltluftturbine des IST*, Auftrag für Siemens Power Generation, Institut für Strahlantriebe und Turboarbeitsmaschinen, RWTH Aachen
[21] Stephan B, Niehuis R and Koschel W 2003 *Experimentelle Untersuchung der Rotorradialspaltströmung in einer $1\frac{1}{2}$-stufigen Axialturbine*, Dissertation RWTH Aachen, Shaker Verlag: Aachen